Original

Razzaq, M.Y.; Behl, M.; Frank, U.; Koetz, J.; Szczerba, W.; Lendlein, A.:

Oligo(Omega-pentadecalactone) decorated magnetic nanoparticles

In: Journal of Materials Chemistry (2012) RSC Publishing

DOI: 10.1039/c2jm16146j

Journal of Materials Chemistry

Cite this: DOI: 10.1039/c2jm16146j

www.rsc.org/materials

PAPER

Oligo(ω-pentadecalactone) decorated magnetic nanoparticles†

Muhammad Yasar Razzaq,[ab] Marc Behl,[a] Ute Frank,[c] Joachim Koetz,[b] Wojciech Szczerba[d] and Andreas Lendlein*[ab]

Received 24th November 2011, Accepted 16th February 2012
DOI: 10.1039/c2jm16146j

Hybrid magnetic nanoparticles (mgNP) with a magnetite core diameter of 10 ± 1 nm surface functionalized with oligo(ω-pentadecalactone) (OPDL) oligomers with M_n between 1300 and 3300 g mol^{-1} could be successfully prepared having OPDL grafted from 200 mg g^{-1} to 2170 mg g^{-1}. The particles are dispersible in chloroform resulting in stable suspensions. Magnetic response against an external magnetic field proved the superparamagnetic nature of the particles with a low coercivity (B_c) value of 297 μT. The combination of the advantageous superparamagnetism of the mgNP with the exceptional stability of OPDL makes these novel hybrid mgNP promising candidates as multifunctional building blocks for magnetic nanocomposites with tunable physical properties.

Introduction

Recently, homo- and multi-block copolymers as well as copolymer networks providing poly(ω-pentadecalactone) (PPDL) segments attracted great interest because of their unique thermal and mechanical properties.[1–6] On the one hand PPDL is an aliphatic polyester, which features the properties of polyethylene (PE) due to the high crystallinity of the aliphatic $C_{14}H_{28}$ unit resulting in a melting temperature (T_m) close to 100 °C (LDPE; T_m = 100–117 °C). Depending on the molecular weight of the PPDL *E*-moduli of up to 420 MPa and elongations at break (ε_b) of more than 1200% could be achieved, which is comparable to those of LDPE.[3] On the other hand, PPDL also provides ester linkages, which could be cleaved.[2,5–10] The ester linkages are relatively stable towards hydrolytical or enzymatic degradation, but could be cleaved when harsher conditions were applied.

When multiblock copolymers were prepared from oligo(ω-pentadecalactone) (OPDL) and poly(ε-caprolactone) (PCL) segments, shape-memory polymers could be obtained.[4] The PCL-segments provided the domains acting as switching domains for fixing the temporary shape, while the OPDL segments provided the hard domains fixing the permanent shape. The copolymerisation of star-shaped hydroxyl-telechelic precursors from PCL and OPDL enabled copolymer networks, in which PCL- and OPDL-segments provided switching domains, resulting in triple-shape materials with the ability to memorize two temporary shapes.[5,6] Such properties would be highly interesting for the design of the surface/interface of nanoparticles.

The incorporation of organic or inorganic particles into shape-memory materials creates multifunctional shape-memory polymers. Of special interest is the incorporation of magnetic nanoparticles (mgNP), which provides nanocomposites combining the advantages of organic polymers (flexibility and processability) with magnetosensitivity.[11] Such nanocomposites can be formed by the incorporation of the mgNP before, during, or after the crosslinking process.[12] However, this physical mixing of mgNP can result at high loading level in loss of elastic properties or material functionality.[13]

At the same time monodispersed mgNP are necessary as the agglomerated nanoparticles formed due to strong magnetic dipole–dipole attraction differ in the magnetic properties from the individual nanoparticles.[14,15] A common strategy to obtain the required properties is the encapsulation of mgNP. Quite frequently, coating with an additional inorganic layer such as silica has been explored.[16,17] Such inorganic coatings can result in a tremendous shielding of the magnetic properties as well as the thermal conductivity of particles. Although the compatibility of the mgNP with the polymer matrix is enhanced, the coated particles still might be repelled from the polymer matrix due to the chemical dissimilarity. Conclusively, another target aimed approach is the surface modification of the mgNP with the polymer, which is also used as a matrix of the nanocomposite, creating magnetite–polymer hybrid nanoparticles.[18–22] An interesting approach would be core–shell mgNP in which the magnetic properties of mgNP are combined with the structural features and mechanical properties of OPDL.

[a]*Centre for Biomaterial Development and Berlin-Brandenburg Center for Regenerative Therapies, Institute of Polymer Research, Helmholtz-Zentrum Geesthacht, Kantstraße 55, D-14513 Teltow, Germany. E-mail: andreas.lendlein@hzg.de*
[b]*Institute of Chemistry, University of Potsdam, D-14476-Potsdam, Germany*
[c]*Helmholtz-Zentrum Potsdam, Deutsches GeoForschungs Zentrum GFZ, D-14473 Potsdam, Germany*
[d]*BAM Federal Institute for Materials Research and Testing, Division 1.3, Structure Analysis, Polymer Analysis, D-12489 Berlin, Germany*
† Electronic supplementary information (ESI) available. See DOI: 10.1039/c2jm16146j

Several routes have been explored to prepare polymer-coated mgNP including (mini)emulsion or dispersion polymerization techniques, adsorption of polymers, as well as surface complexation. The major drawback of all these techniques is the physisorption of the macromolecules on the particle surface, which makes them very sensitive for dissolution and/or depletion.[23–25] A higher stability of the polymeric shell can be reached in the "grafting from" approach as the polymerization is initiated directly from the particle surface resulting in covalently attached polymer chains (Fig. 1). Most "grafting from" approaches require a surface modification with an organic compound acting as an initiator for the subsequent polymerization.[26–30]

Functionalisation of particles in a "grafting from" approach was reported with different types of polymers such as poly(ε-caprolactone),[23,31–33] poly(*rac*-lactides),[28,29] polyethylene oxide,[21,34] polystyrene,[35] poly(methyl methacrylate),[27] and poly(*N*-vinyl pyrrolidone)[36] as well as by different grafting methods. When the particles were functionalized with PE, a hydrophobic surface could be obtained. However, control of the molecular weight of the macromolecules at the particle surface was rather difficult due to the high polymerization rate. Certain control of the molecular weight could be achieved, when the particle surfaces were functionalized by ring-opening polymerization (ROP).[25,31] The obtained polymer surfaces were rather hydrophilic due to the low ratio of methylene groups to ether and ester groups, respectively.

Here, we explored whether mgNP could be functionalized with hydrophobic polymer chain segments by ROP of ω-pentadecalactone (PDL). We sketch the synthesis of the mgNP, investigate a surface functionalisation of the mgNP with PDL, characterise the surface-grafted OPDL, and discuss the influence of the OPDL grafting on the magnetic properties of the mgNP.

Experimental

Materials and methods

Ferric chloride hexa-hydrate ($FeCl_3 \cdot 6H_2O$), ferrous chloride tetra-hydrate ($FeCl_2 \cdot 4H_2O$), ammonium hydroxide (NH_4OH), ω-pentadecalactone (PDL), dibutyltin oxide, and hydrochloric acid were of analytical grade, obtained from Sigma-Aldrich (Munich, Germany), and were used as received. The linear

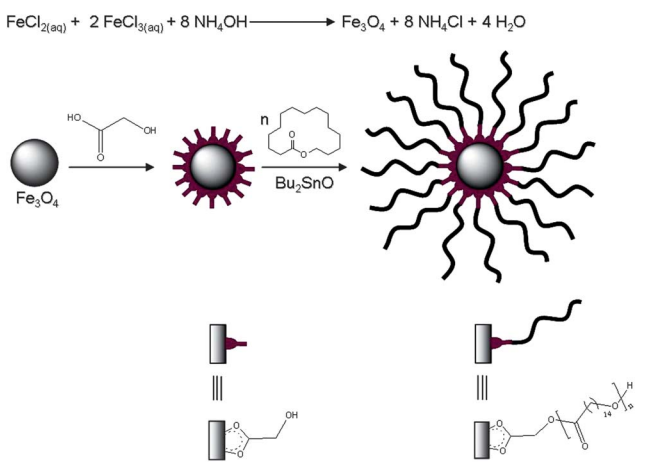

Fig. 1 Synthetic pathway for the preparation of mgNP–OPDL.

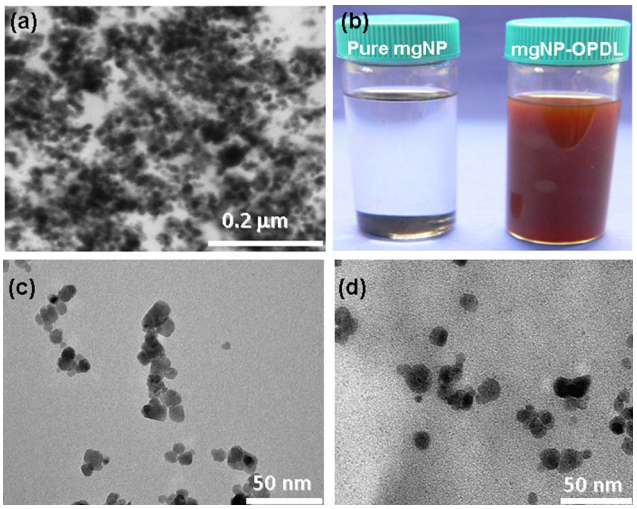

Fig. 2 (a) SEM image of mgNP(1)OPDL(1.9). (b) Photographs of the pure mgNP (left) and OPDL modified mgNP (right) (mgNP(1) OPDL(1.9)) in chloroform taken after 24 h. (c) TEM analysis of the pure mgNP. (d) TEM analysis of the mgNP(1)OPDL(1.9).

$OPDL_r$ (M_n 3900 g mol^{-1}) was obtained by ROP of PDL catalyzed by dibutyltin oxide using hexane diol as an initiator.[4] The OPDL dimethacrylate (OPDL-DMA) (M_n 2800 g mol^{-1}) was prepared by equimolar conversion of terminal hydroxyl groups of OPDL diol (M_n 2700 g mol^{-1}) with 2-isocyanatoethyl methacrylate (IEMA) in 88% yield.

The morphology and size of the particles were determined by Transmission Electron Microscopy (TEM) with a Zeiss EM 902 (Zeiss, Oberkochen, Germany) (ESI, S1†); the morphology of the composite was investigated by Scanning Electron Microscopy (SEM) with a Zeiss Gemini, Supra 40VP (Zeiss, Jena Germany). Hydroxyl groups (OH-numbers) of the particles were determined with a 716 DMS/719 S Titrino titrator system combined with a LiCl-electrode (Metrohm, Filderstadt, Germany). Thermal transitions of OPDL functionalized particles (mgNP–OPDL) were determined by differential scanning calorimetry (DSC) using a DSC 204 Phoenix (Netzsch, Selb, Germany) in a range between −100 °C and 150 °C with a heating rate of 5 °C min^{-1}. FT-IR spectra were recorded from KBr discs prepared from grafted- or non-grafted mgNP on a Nicolet Magna 550 spectrometer. Thermogravimetric analysis (TGA) was conducted on a Netzsch TG209 with a heating rate of 5 K min^{-1} between 25 and 800 °C under a nitrogen purge. Wide angle X-ray scattering (WAXS) measurements were conducted at ambient temperature in reflection mode utilizing a Bruker D8 Discover (Karlsruhe, Germany) X-ray diffraction system with a two-dimensional detector. ^{1}H-NMR spectra were recorded on a 500 MHz advance spectrometer (Bruker, Karlsruhe, Germany) in deuterated chloroform with tetramethylsilane (TMS) as internal standard. M_n of degrafted OPDL was determined by MALDI-TOF using an UltrafleXtreme mass spectrometer (Bruker, Bremen, Germany) (ESI, S1†). M_n of degrafted and linear OPDL was also determined by a multidetector GPC-system using chloroform as eluent (ESI, S1†). The magnetic measurements were performed with a Princeton Measurements Corporation Alternating Gradient Magnetometer (MicroMag™, Princeton, USA) (ESI, S1†). XAFS spectra were measured at the

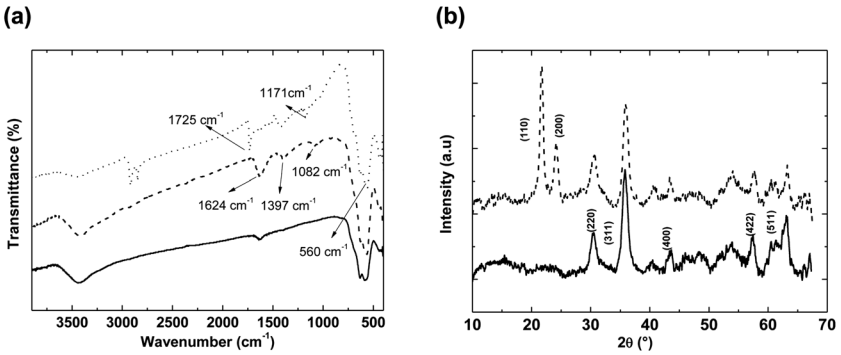

Fig. 3 (a) FT-IR spectra and (b) WAXS analysis; solid line: pure mgNP, dotted line: mgNP–GA, and dashed line: mgNP(1)OPDL(1.9).

μSpot beamline at Bessy II in the XRF mode at the absorption K-edge of Fe (7112 eV) as described in ref. 37.

Synthesis of mgNP

2.07 g $FeCl_3 \cdot 6H_2O$ and 0.81 g $FeCl_2 \cdot 4H_2O$ were dissolved in 100 mL water, which was continuously stirred and N_2 was bubbled in. The solution was heated to 80 °C, 10 mL NH_4OH were added dropwise, and stirred for another 30 min. After 2 h, the black precipitate was collected with a magnet, washed twice with deionized water and thrice with ethanol, and then dried at 60 °C under vacuum until constant weight was achieved.

Synthesis of mgNP–OPDL

mgNP were functionalized with hydroxyl groups by treating the mgNP in an aqueous solution of glycolic acid (GA) with ultrasound for 30 min. The resulting suspension was kept for 12 h at room temperature. The GA functionalized mgNP (mgNP–GA) was then repeatedly washed with 1.3% v/v aqueous NH_4OH to remove free GA. OPDL functionalization of mgNP was achieved by placing mgNP–GA (1 g), PDL (1.93 g), and dibutyltin oxide (0.3 mg) as catalyst in a dried glass flask equipped with a magnetic stirrer and subsequent stirring of the reaction mixture for 21 days at 130 °C. 10 mL chloroform was added to disperse the particles. The uncoated and agglomerated particles were removed by centrifugation (2 min at 1500 rpm) and the supernatant was precipitated into hexane. The formed core–shell nanoparticles mgNP–OPDL were dried in a vacuum oven at 50 °C to constant weight.

Degrafting of OPDL chains from mgNP core

100 mg mgNP–OPDL were dispersed in 10 mL chloroform in a round bottom flask, followed by addition of 1 M aqueous HCl (20 mL).[29] The mixture was stirred vigorously at room temperature until the black color had changed to yellow. The mgNP were separated with the help of a magnet from the organic phase, which was dried overnight above anhydrous $MgSO_4$. The degrafted OPDL was precipitated in hexane and dried in a vacuum until constant weight was achieved (37 mg).

Synthesis of a OPDL-DMA/mgNP–OPDL nanocomposite

0.1 g mgNP(1)OPDL(1.9) and 0.9 g OPDL-DM were vigorously stirred at 100 °C for five minutes, 1.5 mol% dicumyl peroxide were added, and finally cured at 130 °C for 24 h.[38]

Results and discussion

mgNP were prepared by a co-precipitation of aqueous Fe^{+3}/Fe^{+2} in alkaline solution[39] (Fig. 1). The size of the mgNP was confirmed by wide angle X-ray scattering (WAXS) analysis (Fig. 3b), for which an average crystallite size of 10 ± 1 nm was calculated using the Debye–Scherrer equation. As the diameters of the mgNP were well below the critical domain size of magnetite, a superparamagnetic behavior was expected.

The particles were functionalized with hydroxyl groups by chemisorption of GA at the surface of the mgNP, which were suspended in aqueous solution by the application of ultrasound. The content of grafted GA on the mgNP surface determined by TGA was 4 wt% (Fig. 4b). A GA density of 0.53 mmol g^{-1} was calculated (using M GA = 76.05 g mol^{-1}), which was equal to 3.19×10^{20} OH-groups per gram mgNP (equivalent to 860 OH-groups per particle).

The synthesis route for the surface modification is illustrated in Fig. 1. Surface-immobilized hydroxyl groups of mgNP–GA served as initiators for a ROP of PDL in bulk catalyzed by dibutyltin oxide.[40] A reaction time of 21 days was required as the ROP of lactones of a large ring-size (*i.e.* PDL) is less efficient compared to 5- or 7-membered lactones (*i.e.* ε-caprolactone) due to the lower ring strain. The obtained mgNP–OPDL were collected from chloroform solution with the help of a magnet and were dried carefully. In X-ray absorption near edge structure (XANES) investigations conducted at the Fe K-edge of pure mgNP and mgNP–OPDL (ESI, Fig. S3†) no change of the oxidation state of the mgNP after OPDL modification was found.[41]

Morphology and elemental composition of the mgNP–OPDL were studied by SEM equipped with an EDX analyzer. A representative SEM image of mgNP(1)OPDL(1.9) (for sample ID please see footnote a of Table 1) is presented in Fig. 2a showing the mgNP as agglomerated black spots decorated with OPDL (white). In the TEM micrographs (Fig. 2c and d) differently shaped nanoparticles with diameters between 10 and 12 nm can be seen, which is in good agreement with the results from X-ray diffraction. Energy dispersive X-ray (EDX) measurements were conducted (ESI, Fig. S4†) to determine the elements present in the samples. In the EDX the presence of Fe, Cu, O and C was determined, with Cu originating from the copper grid used for the analysis. The agglomeration of C at a similar place compared to the mgNP (Fe distribution) can be attributed to a decoration of the OPDL on the mgNP.

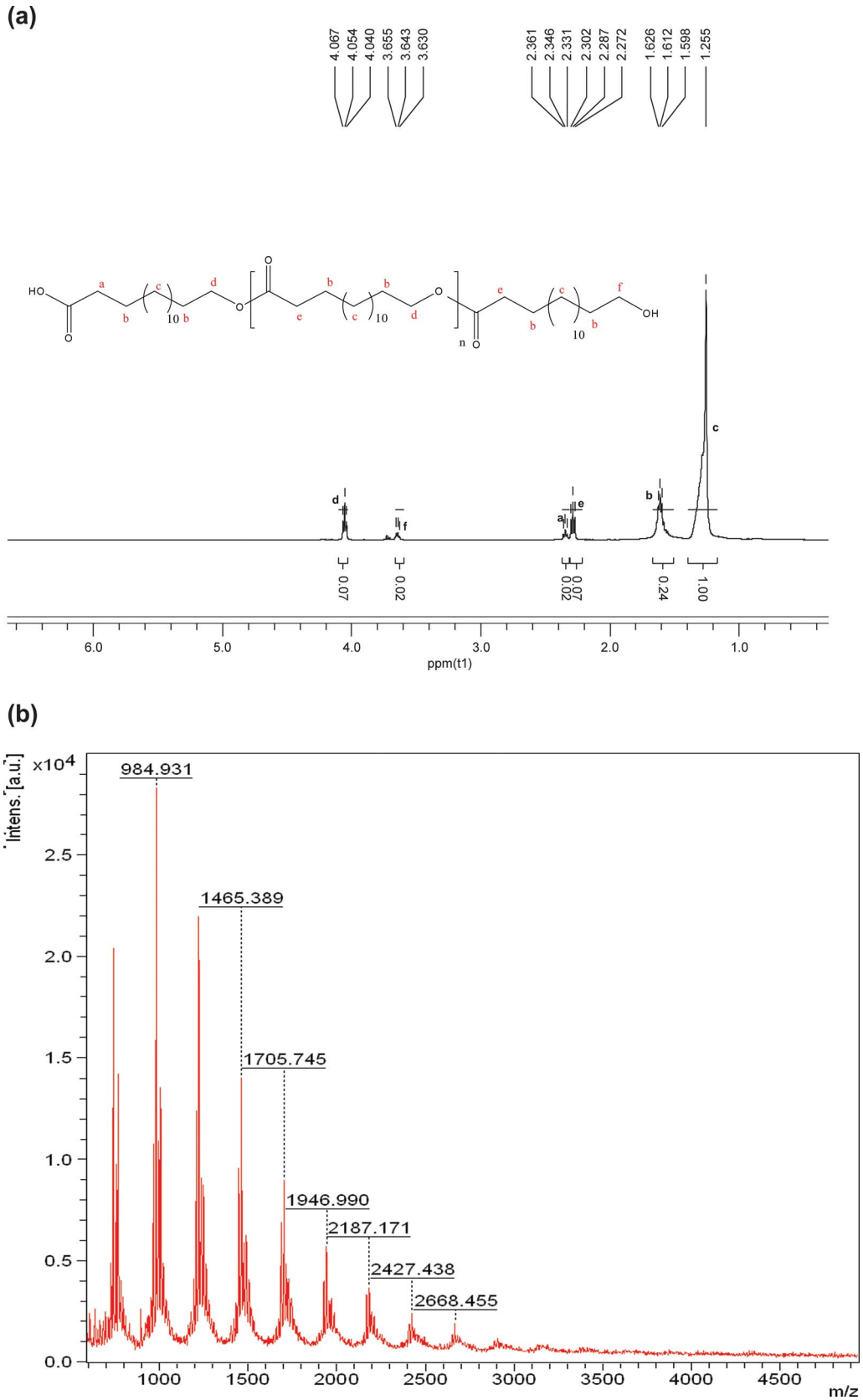

Fig. 4 Characterisation of the degrafted OPDL from mgNP(1)OPDL(0.3) (a) ^{1}H NMR-spectra and (b) MALDI-TOF-MS spectra.

Table 1 Properties of the hybrid mgNP grafted with different OPDL chain lengths

Sample no.[a]	M_n[b]/g mol^{-1}	M_n[c]/g mol^{-1}	PDI[d]	T_m[e]/°C	G[f]/mg g^{-1}
mgNP(1)OPDL(0.3)	1282	800	3.1	70	200
mgNP(1)OPDL(0.7)	1283	1000	3.6	78	458
mgNP(1)OPDL(1.0)	1345	1100	2.9	83	1288
mgNP(1)OPDL(1.9)	2200	2200	3.2	87	2170

[a] mgNP(x)OPDL(y) where x and y are the amounts of mgNP–GA and PDL in grams used during surface-initiated ROP. [b] Number average molecular weight determined by MALDI-TOF MS. [c] Number average molecular weight determined by ^{1}H NMR. [d] Polydispersity index determined by standard calibrated multi-detector GPC. [e] Melting temperature determined by DSC. [f] Grafting density determined by eqn (1).

The OPDL shell served as the stabilizing component preventing particle agglomeration due to the magnetic dipole–dipole attractive forces. Suspensions made from mgNP–OPDL and chloroform were stable for several weeks (Fig. 2b), indicating the successful grafting with OPDL chains. In contrast, the suspension of pure mgNP precipitated only after a few minutes without stirring. When a separately prepared linear OPDL was dissolved in chloroform and pure mgNP were added to this solution, sedimentation of the particles occurred within 1 h. This indicates that an effective stabilization of the mgNP required covalently attached polymeric chains. When the mgNP–OPDL was suspended in other high boiling solvents such as dioxane or DMSO the dispersion was stable above $T_{m,OPDL}$ but the mgNP–OPDL precipitated below $T_{m,OPDL}$ (ESI, S2†).

The evidence of the GA and OPDL on the surface of mgNP was confirmed by FT-IR analysis. Fig. 3a shows the FT-IR analysis of the pure mgNP, mgNP–GA, and mgNP–OPDL respectively. The intense band located at 560 cm^{-1} corresponds to the stretching vibration mode of Fe–O bonds in magnetite. The chemisorption of the carboxylate functionality on the surface of mgNP was confirmed by the appearance of COO^- symmetric (sym, 1397 cm^{-1}) and asymmetric (asym, 1624 cm^{-1}) stretching vibration bands, while the vibration of C=O at 1702 cm^{-1} in the free GA disappeared.[42,43] Meanwhile, the absorption of the alcoholic C–OH bond of free GA (1082 cm^{-1}) did not show any significant change in the spectrum of mgNP–GA, which provided the possibility that polymerization of the PDL monomer could be initiated directly from the surface of mgNP. Compared to mgNP, a new absorption band appeared at 1725 cm^{-1} for mgNP–OPDL, which was attributed to the C=O group of OPDL at the surface of mgNP. Other bands observed between 1000 and 1500 cm^{-1} can be assigned to the C–O and C–C stretching in OPDL. The strong bands associated with the asymmetric and symmetric $-CH_2-$ stretching vibration were observed at 2918 and 2843 cm^{-1}.[25,31]

The WAXS analysis confirmed the presence of two crystalline phases from mgNP and OPDL (Fig. 3b). For pure mgNP, the position and relative intensities of all peaks match well with the known pattern of crystalline magnetite.[36,44] The characteristic diffraction peaks (220), (311), (400), (422), and (511) can be assigned to the inverse cubic spinel structure of magnetite. In addition to these peaks, mgNP–OPDL displayed peaks (110) and (200) at $2\theta = 21.7°$ and 24.2° corresponding to the crystalline structure of OPDL.[23] No change in the position or intensity of the peaks assigned to the mgNP was observed after coating with OPDL.

For further characterization of the polymeric shell, the polymer chains were cleaved from the nanoparticles by acidolysis with dilute HCl and separated from the mgNP. A linear OPDL ($M_n = 3900$ g mol^{-1}) diol used as reference material ($OPDL_r$) was treated similarly to ensure that no significant change of the molecular weight or the distribution occurred, and in this way to prove the absence of polyester degradation during shell cleavage under the applied acidic conditions.

The structure of the cleaved OPDL was determined by ^{1}H-NMR (Fig. 4a) and was consistent with the reported spectra of OPDL.[7] ^{1}H NMR (500 MHz, $CDCl_3$, δ): 3.99 (t, CH_2^aO), 3.58 (t, CH_2^eOH), 2.27 (t, CH_2^b–CO), 1.55, 1.18 (m, $CH_2^{c,d}$), 4.16 (s, CH_2^f–). The small peak at 4.16 was assigned to the methylene group of the terminal GA moiety.

The molecular weight of the isolated polymeric chains was investigated by matrix-assisted laser desorption/ionization

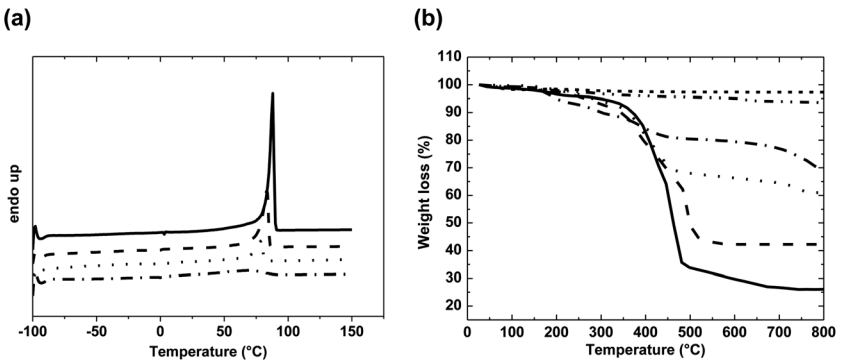

Fig. 5 (a) DSC spectra of mgNP–OPDL and (b) TGA curves; short-dashed line: pure mgNP, dash-dot-dotted line: mgNP–GA, dash-dotted line: mgNP(1)OPDL(0.3), dotted line: mgNP(1)OPDL(0.7), dashed line: mgNP(1)OPDL(1.0), and solid line: mgNP(1)OPDL(1.9).

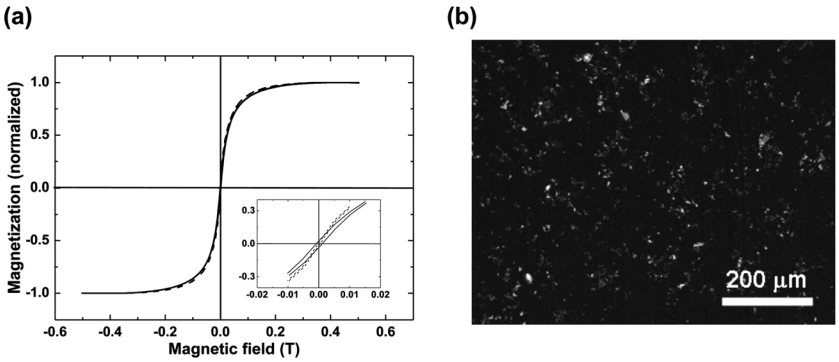

Fig. 6 (a) Magnetization curves. The inset enlarges the center of the hysteresis loops (solid line: pure mgNP and dashed line: mgNP(1)OPDL(1.9)). (b) SEM image of the OPDL nanocomposite containing 10 wt% of mgNP(1)OPDL(1.9).

time-of-flight mass spectrometry (MALDI-TOF-MS) and ^{1}H-NMR spectroscopy. In ^{1}H-NMR measurements the number average molecular weight (M_n) was calculated using the equation $M_n = (I_a/I_e) \times 240 + 59$, where ($I_d/I_f$) is the ratio of the intensity of signal "d" attributed to the methylene protons of the repeat unit (t, $\delta = 3.99$) to the signal "f" corresponding to the methylene protons next to the hydroxyl end groups (t, $\delta = 3.64$) and 240 and 59 are the molar masses of the PDL and GA. The M_n of the isolated OPDLs determined by MALDI-TOF MS fitted well with the results obtained by ^{1}H-NMR and were in the range between 2200 g mol^{-1} and 1280 g mol^{-1}. A unimodal molecular weight distribution was observed with a mass difference of 240 between the peaks, which correlated with the molecular weight of one PDL unit (Fig. 4b). The polydispersity PDI was determined by GPC and ranged between 2.9 and 3.6 (Table 1).

The thermal properties of the mgNP–OPDL were investigated by DSC and were compared with those of the OPDL$_r$. All samples displayed a well-defined melting transition (T_m) and crystallization temperature (T_c) (Fig. 5a). According to the DSC data, the T_ms of different mgNP–OPDL were lower than those of linear OPDL$_r$ ($T_m = 99$ °C), which was attributed to a higher M_n of the OPDL$_r$ as well as hydrogen bonds due to the hydroxy-telechelic diol structure. Both the T_m and the T_c of mgNP–OPDL increased with increasing length of the grafted OPDL chains (Table 1), which was attributed to the imperfect crystallization behaviour of the grafted OPDL with low molecular weight. In addition, the T_m of the linear OPDL cleaved from the surface of the particles was slightly higher than the T_m of the mgNP–OPDL and can be explained with a higher tendency of crystallization due to the hydrogen bonds of the GA end groups. *E.g.*, the grafted sample mgNP(1)OPDL(1.9) displayed a T_m at 87 °C while the T_m of the cleaved OPDL was 90 °C.

The amount of grafted OPDL chains was quantitatively determined by TGA (Fig. 5b). The materials were heated under nitrogen in a TGA furnace past the point of thermal degradation of the OPDL from which only the magnetite/maghemite was obtained as residual mass. At elevated temperatures, the organic shell of the mgNP–OPDL was completely combusted to gaseous products. The absolute weight loss of the pure mgNP was 3 wt% over the whole temperature range attributed to the loss of physically and chemically adsorbed water. For mgNP–GA, the weight loss increased to 7 wt% at 800 °C, with a significant weight reduction around 160 °C, which was attributed to the decomposition of GA at the surface of mgNP. mgNP–OPDL displayed two decomposition regions: the first one was again at around 160 °C, the second region (onset at ~350 °C) was attributed to the decomposition of OPDL. The weight content of the surface-grafted OPDL was determined as the difference between the weight loss of OPDL- and GA-functionalized nanoparticles [M(OPDL) = W(mgNP–OPDL) − W(mgNP–GA)].[40] The weight content of the surface-grafted OPDL increased from 24 wt% to 67 wt% when the mgNP–GA : PDL feed ratio was increased from 1 : 0.3 to 1 : 1.9 (Fig. 3b). The grafting density (G) of the mgNP–OPDL was calculated from the OPDL weight loss from TGA and the molecular weight was determined by ^{1}H NMR analysis using eqn (1):[32]

$$G(\text{mg g}^{-1}) = \left(\frac{\Delta}{100 - \Delta} - W_{\text{mgNP–GA}}\right) \times 1000 \qquad (1)$$

where Δ (wt%) corresponds to the TGA weight loss between 100 and 600 °C and $W_{\text{mgNP–GA}}$ is the amount of grafted GA in gram per g mgNP. G increased from 200 mg g^{-1} to 2170 mg g^{-1} when M_n of the surface-grafted OPDL was increased from 800 g mol^{-1} to 2200 g mol^{-1} (Table 1). The grafting density was also calculated by OH-group determination by potentiometric titrations, which resulted in G ranging from 128 mg g^{-1} to 782 mg g^{-1}. These values were slightly lower than the values obtained by eqn (1). However, the increasing trend in G with the increase in the molar mass of the surface-grafted OPDL was maintained.

The influence of the OPDL surface grafting on the magnetic properties was explored. The magnetization curves of the pure mgNP and mgNP–OPDL are shown in Fig. 6a. Both samples exhibited a superparamagnetic behaviour at ambient temperature, as evidenced by the steep rise of the curves, which are saturating at low fields. The values of the coercivity (B_c) for mgNP–OPDL (297 μT) was less than that of the pure mgNP (959 μT), attributed to the non-magnetic OPDL coated on the surface of mgNP. The B_c values for all samples were very low and no obvious hysteresis was observed. This indicated that in their natural state the magnetic moments of the domains were oriented randomly, but in the presence of an external magnetic field, the magnetic moments were aligned along the field. As a result, the magnetic susceptibility of a system containing such superparamagnetic nanoparticles usually far exceeds those of paramagnetic materials.[21] Indeed, the OPDL coating did not significantly change the strong saturation magnetization of the

mgNP and the superparamagnetic behaviour, highly useful for biomedical applications, was well preserved.

In a preliminary experiment a nanocomposite was prepared by incorporating 10 wt% of mgNP(1)OPDL(1.9) in a OPDL-DMA, which was subsequently crosslinked. SEM clearly demonstrated an efficient dispersion of the mgNP–OPDL in the OPDL-DMA matrix (Fig. 6b), which was attributed to a much higher compatibility of mgNP–OPDL compared to mgNP.

Conclusion

The creation of magnetic core–shell nanoparticles is a topic of high relevance as such particles find application in nanocomposites or hyperthermia. In this context we explored the surface grafting of mgNP with highly crystallizable and hydrophobic OPDL by surface initiated ROP of PDL. Different mgNP : PDL feed ratios resulted in surface grafting of OPDL with M_n ranging from 1300 g mol^{-1} to 3300 g mol^{-1}. A core–shell structure with a mgNP size between 10 and 12 nm and covalent attachment of the OPDL chains could be proven by TEM, FT-IR, and solution experiments. In chloroform the mgNP–OPDL formed stable dispersions. When other high boiling organic solvents such as dioxane or DMSO were selected, the dispersion was stable above $T_{m,OPDL}$ but the mgNP–OPDL precipitated below $T_{m,OPDL}$. The superparamagnetic behaviour of mgNP–OPDL shown by magnetization experiments makes them ideal candidates for *e.g.* biomedical applications, as these require a high saturation magnetization.

Acknowledgements

The authors gratefully acknowledge beamtime at BESSY II at the 7T-WLS-1 BAMline and thank Prof. Dr Andreas Thünemann for discussion of XAFS measurements as well as Dr Ulrich Nöchel for WAXS investigations.

References

1 B. Kalra, A. Kumar, R. A. Gross, M. Baiardo and M. Scandola, *Macromolecules*, 2004, **37**, 1243–1250.
2 I. van der Meulen, M. de Geus, H. Antheunis, R. Deumens, E. A. J. Joosten, C. E. Koning and A. Heise, *Biomacromolecules*, 2008, **9**, 3404–3410.
3 M. de Geus, I. van der Meulen, B. Goderis, K. van Hecke, M. Dorschu, H. van der Werff, C. E. Koning and A. Heise, *Polym. Chem.*, 2010, **1**, 525–533.
4 K. Kratz, U. Voigt, W. Wagermaier and A. Lendlein, *Mater. Res. Soc. Symp. Proc.*, 2009, **1140**, 17–22.
5 J. Zotzmann, M. Behl, Y. K. Feng and A. Lendlein, *Adv. Funct. Mater.*, 2010, **20**, 3583.
6 J. Zotzmann, M. Behl, D. Hofmann and A. Lendlein, *Adv. Mater.*, 2010, **22**, 3424.
7 M. L. Focarete, M. Scandola, A. Kumar and R. A. Gross, *J. Polym. Sci., Part B: Polym. Phys.*, 2001, **39**, 1721.
8 I. van der Meulen, E. Gubbels, S. Huijser, R. Sablong, C. E. Koning, A. Heise and R. Duchateau, *Macromolecules*, 2011, **44**, 4301–4305.
9 L. Mazzocchetti, M. Scandola and Z. Jiang, *Macromolecules*, 2009, **42**, 7811–7819.
10 M. Behl, J. Zotzmann and A. Lendlein, *Int. J. Artif. Organs*, 2011, **34**, 231.
11 H. Althues, J. Henle and S. Kaskel, *Chem. Soc. Rev.*, 2007, **36**, 1454–1465.
12 A. Sanchez-Ferrer, M. Reufer, R. Mezzenga, P. Schurtenberger and H. Dietsch, *Nanotechnology*, 2010, **21**, 185603.
13 R. Fuhrer, E. K. Athanassiou, N. A. Luechinger and W. J. Stark, *Small*, 2009, **5**, 383–388.
14 Y. Zhang, C. Sun, N. Kohler and M. Q. Zhang, *Biomed. Microdevices*, 2004, **6**, 33–40.
15 D. S. Achilleos and M. Vamvakaki, *Materials*, 2010, **3**, 1981–2026.
16 Y.-H. Deng, C.-C. Wang, J.-H. Hu, W.-L. Yang and S.-K. Fu, *Colloids Surf., A*, 2005, **262**, 87–93.
17 A.-H. Lu, E. L. Salabas and F. Schüth, *Angew. Chem., Int. Ed.*, 2007, **46**, 1222–1244.
18 J. Kim, H. S. Kim, N. Lee, T. Kim, H. Kim, T. Yu, I. C. Song, W. K. Moon and T. Hyeon, *Angew. Chem., Int. Ed.*, 2008, **47**, 8438.
19 B. Kiskan, A. L. Demirel, O. Kamer and Y. Yagci, *J. Polym. Sci., Part A: Polym. Chem.*, 2008, **46**, 6780.
20 M. Koneracka, V. Zavisova, M. Timko, P. Kopcansky, N. Tomasovicova and K. Csach, *Acta Phys. Pol., A*, 2008, **113**, 595.
21 M. Mahmoudi, A. Simchi, M. Imani and U. O. Hafeli, *J. Phys. Chem. C*, 2009, **113**, 8124.
22 M. Omer, S. Haider and S. Y. Park, *Polymer*, 2011, **52**, 91.
23 C. Flesch, E. Bourgeat-Lami, S. Mornet, E. Duguet, C. Delaite and P. Dumas, *J. Polym. Sci., Part A: Polym. Chem.*, 2005, **43**, 3221.
24 L. L. Zhou, J. M. Kuang and J. Y. Yuan, *Prog. Chem.*, 2009, **21**, 1880.
25 L. L. Zhou, J. Y. Yuan, W. Z. Yuan, M. Zhou, S. Z. Wu, Z. L. Li, X. H. Xing and D. Z. Shen, *Mater. Lett.*, 2009, **63**, 1567.
26 A. P. Herrera, M. Rodriguez, M. Torres-Lugo and C. Rinaldi, *J. Mater. Chem.*, 2008, **18**, 855.
27 E. Marutani, S. Yamamoto, T. Ninjbadgar, Y. Tsujii, T. Fukuda and M. Takano, *Polymer*, 2004, **45**, 2231.
28 J. Tian, Y. K. Feng and Y. S. Xu, *Macromol. Res.*, 2006, **14**, 209.
29 J. Tian, Y. K. Feng and Y. S. Xu, *J. Polym. Res.*, 2006, **13**, 343.
30 W. Z. Yuan, J. Y. Yuan, L. L. Zhou, S. Z. Wu and X. Y. Hong, *Polymer*, 2010, **51**, 2540.
31 A. Nan, R. Turcu, I. Craciunescu, O. Pana, H. Scharf and J. Liebscher, *J. Polym. Sci., Part A: Polym. Chem.*, 2009, **47**, 5397.
32 C. Flesch, C. Delaite, P. Dumas, E. Bourgeat-Lami and E. Duguet, *J. Polym. Sci., Part A: Polym. Chem.*, 2004, **42**, 6011.
33 J. Yang, S. B. Park, H.-G. Yoon, Y. M. Huh and S. Haam, *Int. J. Pharm.*, 2006, **324**, 185–190.
34 F. X. Hu, K. G. Neoh, L. Cen and E. T. Kang, *Biomacromolecules*, 2006, **7**, 809.
35 R. Matsuno, K. Yamamoto, H. Otsuka and A. Takahara, *Macromolecules*, 2004, **37**, 2203–2209.
36 N. Arsalani, H. Fattahi and M. Nazarpoor, *eXPRESS Polym. Lett.*, 2010, **4**, 329.
37 J. Polte, T. T. Ahner, F. Delissen, S. Sokolov, F. Emmerling, A. F. Thünemann and R. Kraehnert, *J. Am. Chem. Soc.*, 2010, **132**, 1296–1301.
38 M. Y. Razzaq, M. Behl and A. Lendlein, *Mater. Res. Soc. Symp. Proc.*, 2012, DOI: 10.1557/opl.2012.222.
39 R. Massart and V. Cabuil, *J. Chim. Phys.*, 1987, **84**, 967.
40 F. H. Chen, Q. Gao, G. Y. Hong and J. Z. Ni, *J. Magn. Magn. Mater.*, 2008, **320**, 1921.
41 M. C. Urbina, S. Zinoveva, T. Miller, C. M. Sabliov, W. T. Monroe and C. S. S. R. Kumar, *J. Phys. Chem. C*, 2008, **112**, 11102–11108.
42 A. Drmota, A. Kosak and A. Znidarsic, *Mater. Tehnol.*, 2008, **42**, 79.
43 A. I. Lesnikovich, T. M. Shunkevich, V. N. Naumenko, S. A. Vorobyova and M. V. Baykov, *J. Magn. Magn. Mater.*, 1990, **85**, 14–16.
44 L. Zhang, R. He and H. C. Gu, *Appl. Surf. Sci.*, 2006, **253**, 2611.